J. Fluid Mech. (2009), *vol.* 620, *pp.* 177–194.
doi:10.1017/S0022112008004631 Printed in the United Kingdom

Homogenized Euler equation: a model for compressible velocity gradient dynamics

S. SUMAN† AND S. S. GIRIMAJI

Department of Aerospace Engineering, Texas A&M University, College Station, TX 77843-3141, USA
girimaji@aero.tamu.edu

(Received 22 March 2008 and in revised form 10 October 2008)

Along the lines of the restricted Euler equation (REE) for incompressible flows, we develop homogenized Euler equation (HEE) for describing turbulent velocity gradient dynamics of an isentropic compressible calorically perfect gas. Starting from energy and state equations, an evolution equation for pressure Hessian is derived invoking uniform (homogeneous) velocity gradient assumption. Behaviour of principal strain rates, vorticity vector alignment and invariants of the normalized velocity gradient tensor is investigated conditioned on dilatation level. The HEE results agree very well with the known behaviour in the incompressible limit. Indeed, at zero dilatation HEE reproduces the incompressible anisotropic pressure Hessian behaviour very closely. When compared against compressible direct numerical simulation results, the HEE accurately captures the strain rate behaviour at different dilatation levels. The model also recovers the fixed point behaviour of pressure-released (high-Mach-number limit) Burgers turbulence.

1. Introduction

Examination of velocity gradient dynamics is crucial to understanding important turbulence phenomena such as energy cascade, scalar mixing, material element deformation and intermittency. The magnitude and sign of the principal strain rates reveal the nature of self-straining of a fluid element. Orientation of the vorticity vector with respect to the eigendirections of the strain rate tensor and the pressure Hessian tensor influences energy cascade rate (Ohkitani 1993). Alignment of vorticity with the eigenvector along a positive strain rate corresponds to vortex stretching whereas orientation with the eigenvector of a negative principal strain rate represents vortex compression. Scalar gradients are steepened leading to enhanced mixing, when aligned along a negative principal strain rate. The phenomenon of intermittency is directly related to the localized magnification of velocity gradients (Li & Meneveau 2005). The topology of the local velocity field near a critical point can be visualized with knowledge of the invariants of velocity gradient tensor (Perry & Chong 1987; Chong, Perry & Cantwell 1990). It is desirable to develop a simple dynamical model to capture the essential features of velocity gradient physics in turbulent flows. Such a model can also serve as the basis of stochastic turbulence closures (Girimaji & Pope 1990).

Velocity gradient evolution is dictated principally by nonlinear processes. Linear analytical theories of turbulence – like the rapid distortion theory (RDT) – are

† Email address for correspondence: sawan@tamu.edu

thus not applicable. Based on the Euler equation, an autonomous system of ordinary differential equations – called the restricted Euler equation (REE) – was proposed by Vieillefosse (1982) to describe the nonlinear velocity gradient dynamics in incompressible flows. Ashurst *et al.* (1987) demonstrated that REE accurately captures many important features of velocity gradient geometry including the alignment of vorticity with strain rate eigenvectors. Subsequently, several modifications have been proposed to enhance the REE. Cantwell (1992) presented invariant maps of velocity gradient tensor to develop more insight into the tensor geometry. Cantwell (1993) also proposed an anisotropic pressure Hessian closure that captures some additional features of the invariants seen in direct numerical simulation (DNS) results. Girimaji & Speziale (1995) identified a limitation in the original REE in the context of non-zero mean flows and proposed modified REE to ensure momentum conservation. Also a computational strategy to circumvent the problem of finite-time singularity was developed. Chertkov, Pumir & Shraiman (1999) proposed an improvement to REE based on Lagrangian tetrad dynamics. Jeong & Girimaji (2003) incorporated further physics into the REE to take into account the viscous effects and consequently removing the finite-time singularity problem altogether. Recently, Li & Meneveau (2005) have used the restricted Euler dynamics to propose a simple nonlinear dynamical model to explain the origins of intermittency in turbulent flows. Chevillard & Meneveau (2006) have also suggested modifications to capture the effects of the neglected viscous and anisotropic pressure Hessian terms. Overall, REE is emerging as an important analytical tool – a nonlinear counterpart of RDT – for studying various turbulence mechanisms. REE and RDT address different aspects of turbulence dynamics and, hence, are mutually exclusive in terms of physics content.

The interaction of pressure with velocity field plays an important role in velocity gradient dynamics. In incompressible flows the pressure field depends exclusively upon velocity field via the Poisson equation. The restricted Euler model takes advantage of this fact and closes the pressure Hessian in terms of the velocity gradient itself by completely neglecting the anisotropic portion of the tensor. In compressible flows the pressure field evolution is dictated by state and energy equations. Variations in temperature and density manifest on the turbulent velocity field via pressure effects. The momentum and energy equations become coupled, and thermodynamics can significantly influence the velocity field. A velocity gradient model for compressible flow field must necessarily take into account this coupling between turbulence and thermodynamics. The REE approximation, which hinges on Poisson equation, is fundamentally unsuited for extension to compressible flows.

Our principal objective is to develop a velocity gradient model for turbulent compressible flows along the lines of the incompressible REE model. We derive such a model from energy and state equations by invoking uniform velocity gradient assumption (Vieillefosse 1982). Then, we seek to establish the validity of the model by comparing: (i) the asymptotic behaviour against fixed points of Burgers turbulence (Bikkani & Girimaji 2007); (ii) the incompressible-limit behaviour against incompressible DNS results (Ashurst *et al.* 1987; Soria *et al.* 1994) and (iii) strain rate statistics at intermediate dilatations against compressible DNS results (Lee 2008). We also make comparisons with the asymptotic REE results to highlight the improvements achieved in the incompressible limit.

We develop the model – homogenized Euler equation (HEE) – in § 2. Section 3 contains a discussion of the numerical method and establishes the various velocity gradient statistics of interest. In § 4 we present the model results and evaluate the

performance of the model against known turbulence behaviour. Section 5 concludes the paper with a summary.

2. Homogenized Euler equation

In this section we develop the homogenized Euler equation and highlight the involved assumptions. For an inviscid calorically perfect gas without any heat source, the conservation of mass, momentum and energy equations are

$$\frac{\partial \rho}{\partial t} + \frac{\partial (\rho V_k)}{\partial x_k} = 0, \tag{2.1}$$

$$\frac{\partial V_i}{\partial t} + V_k \frac{\partial V_i}{\partial x_k} = -\frac{1}{\rho}\frac{\partial p}{\partial x_i}, \tag{2.2}$$

$$\frac{\partial T}{\partial t} + V_k \frac{\partial T}{\partial x_k} = -T(n-1)\frac{\partial V_i}{\partial x_i}, \tag{2.3}$$

where n is the ratio of specific heats; V_i, p, ρ and T represent velocity, pressure, density and temperature, respectively. For a perfect gas the three thermodynamic variables are related through the following state equation:

$$p = \rho R T. \tag{2.4}$$

Any attempt to formulate a velocity gradient model for a general perfect gas flow field would lead to a very high degree of complexity. As a first step we restrict our consideration to a flow field which has a uniform entropy distribution. With this assumption the state equation (2.4) simplifies to the following form:

$$p = C\rho^n, \tag{2.5}$$

where C is constant both in time and space. This assumption significantly simplifies the formulation and yet captures the influence of a thermodynamically evolving pressure field on velocity gradient dynamics. In later works we will ease the uniform entropy assumption to develop models for more complex flows. Nonetheless, we will compare the model performance against decaying non-isentropic turbulence data to investigate the practical utility of the new model. We will also compare the model against Burgers turbulence which represents an extreme limit of compressible flow.

2.1. *Equation for the velocity gradients*

We now derive the evolution equation for the primary quantity of interest, the velocity gradient tensor $\boldsymbol{A}_{ij}$

$$\boldsymbol{A}_{ij} \equiv \frac{\partial V_i}{\partial x_j}. \tag{2.6}$$

Equation (2.2) is re-written using (2.5) as

$$\frac{\partial V_i}{\partial t} + V_k \frac{\partial V_i}{\partial x_k} = -\frac{1}{\rho}\frac{\partial (C\rho^n)}{\partial x_i}. \tag{2.7}$$

Taking gradient of this equation leads to an equation for $\boldsymbol{A}_{ij}$:

$$\frac{\mathrm{d}\boldsymbol{A}_{ij}}{\mathrm{d}t} = -\boldsymbol{A}_{ik}\boldsymbol{A}_{kj} - \frac{\partial}{\partial x_j}\left(\frac{1}{\rho}\frac{\partial (C\rho^n)}{\partial x_i}\right), \tag{2.8}$$

where $\mathrm{d}/\mathrm{d}t$ indicates material derivative. Now, with C and n being constants the pressure Hessian $\partial((1/\rho)(\partial(C\rho^n)/\partial x_i))/\partial x_j$, simplifies to a symmetric form

$$\frac{\mathrm{d}\boldsymbol{A}_{ij}}{\mathrm{d}t} = -\boldsymbol{A}_{ik}\boldsymbol{A}_{kj} - \frac{Cn}{n-1}\frac{\partial^2 g}{\partial x_i \partial x_j}, \tag{2.9}$$

where $g \equiv \rho^{n-1}$. Closure equation for this symmetric pressure Hessian is next obtained from the mass conservation Equation (2.1):

$$\frac{\mathrm{d}}{\mathrm{d}t}\left(\frac{\partial g}{\partial x_i}\right) = -\boldsymbol{A}_{ki}\frac{\partial g}{\partial x_k} - (n-1)\boldsymbol{A}_{kk}\frac{\partial g}{\partial x_i} - (n-1)g\frac{\partial \boldsymbol{A}_{kk}}{\partial x_i}, \tag{2.10}$$

$$\begin{aligned}\frac{\mathrm{d}}{\mathrm{d}t}\left(\frac{\partial^2 g}{\partial x_i \partial x_j}\right) = &-\boldsymbol{A}_{kj}\frac{\partial^2 g}{\partial x_i \partial x_k} - \boldsymbol{A}_{ki}\frac{\partial^2 g}{\partial x_k \partial x_j} - \frac{\partial \boldsymbol{A}_{ki}}{\partial x_j}\frac{\partial g}{\partial x_k} - (n-1)\boldsymbol{A}_{kk}\frac{\partial^2 g}{\partial x_i \partial x_j} \\ &- (n-1)\frac{\partial \boldsymbol{A}_{kk}}{\partial x_i}\frac{\partial g}{\partial x_j} - (n-1)\frac{\partial \boldsymbol{A}_{kk}}{\partial x_j}\frac{\partial g}{\partial x_i} - (n-1)\frac{\partial^2 \boldsymbol{A}_{kk}}{\partial x_i \partial x_j}g.\end{aligned} \tag{2.11}$$

2.2. *Central assumption of HEE*

As discussed in § 1, it is our objective to construct a simple autonomous dynamical system of equations which can capture the essential features of nonlinear velocity gradient dynamics in compressible turbulence. The success of REE for incompressible flows clearly demonstrates that much insight can be obtained in homogeneous systems wherein the velocity gradients are constant in space (Vieillefosse 1982):

$$\frac{\partial \boldsymbol{A}_{ij}}{\partial x_k} \equiv 0. \tag{2.12}$$

This is the central assumption of our model. Subject to this assumption (2.9) and (2.11) simplify substantially to

$$\frac{\mathrm{d}\boldsymbol{A}_{ij}}{\mathrm{d}t} = -\boldsymbol{A}_{ik}\boldsymbol{A}_{kj} - \boldsymbol{P}_{ij}, \tag{2.13}$$

$$\frac{\mathrm{d}\boldsymbol{P}_{ij}}{\mathrm{d}t} = -\boldsymbol{P}_{ik}\boldsymbol{A}_{kj} - \boldsymbol{P}_{kj}\boldsymbol{A}_{ki} - (n-1)\,\boldsymbol{P}_{ij}\boldsymbol{A}_{kk}, \tag{2.14}$$

where

$$\boldsymbol{P}_{ij} \equiv \frac{Cn}{n-1}\frac{\partial^2 g}{\partial x_i \partial x_j} \tag{2.15}$$

is the pressure Hessian tensor. Equations (2.13) and (2.14) form a closed set of 15 ordinary differential equations in 15 unknowns. We refer to this equation set as the HEE model. It is important here to point out major differences between the HEE and REE formulations. The original REE invokes a more serious assumption in which the pressure Hessian is simplified to only its isotropic component:

$$\frac{\partial}{\partial x_j}\left(\frac{1}{\rho}\frac{\partial p}{\partial x_i}\right) = \frac{1}{\rho}\frac{\partial^2 p}{\partial x_i \partial x_j} = -\frac{\boldsymbol{A}_{mn}\boldsymbol{A}_{nm}}{3}\delta_{ij}. \tag{2.16}$$

This assumption is invoked for the mathematical benefit of yielding a closed set of equations. It must be pointed out that the term 'homogenized' in HEE does not indicate any homogenization procedure. Here, homogeneous refers to the fact that the velocity gradients are (nearly) invariant in space. Homogenization procedure on

the other hand refers to the mathematical limit of setting the heterogeneity scale to infinity, thus rendering the problem homogeneous.

Some attempts have been made in literature to include anisotropic contributions (Cantwell 1993; Chevillard & Meneveau 2006) in REE. These involve other assumptions which have their own limitations. The HEE, on the other hand, does not require any further assumptions regarding the pressure Hessian. The full Hessian in its natural form is included in the model. This is possible due to the invocation of state and energy equations, which are not used in the REE.

2.3. *Velocity gradient dynamics in Burgers turbulence*

In the context of nonlinear turbulence processes, it is relevant to mention the significance of Burgers equation. Burgers turbulence represents the extreme state of compressible turbulence in which pressure effects are negligible in comparison with the inertial effects. For this reason Burgers turbulence is also called the pressure-released turbulence. Burgers turbulence is known (Passot & Vzquez-Semadeni 1998) to provide a reasonably accurate representation of very high-Mach-number Navier–Stokes turbulence in (i) high-density flows with polytropic index less than unity and (ii) low-density flows with polytropic index larger than unity. Due to its simplicity, Burgers equation is often used as a test bed to evaluate new turbulence theories (Avellaneda, Ryan & Weinan 1995; Bouchaud & Mzard 1996). Burgers turbulence also captures some important aspects of the energy cascade mechanism and intermittency seen in Navier–Stokes turbulence. Girimaji & Zhou (1995) demonstrate that the spectral energy transfer and the triadic interactions displayed by Burgers equation are similar to that in Navier–Stokes turbulence. Recently, Bikkani & Girimaji (2007) investigated the dynamics of three-dimensional Burgers equation to probe the role of pressure in incompressible flows. One key result of Bikkani & Girimaji (2007) is that Burgers-turbulence velocity gradients exhibit two stable fixed point families given by

$$(\alpha, \beta, \gamma, \omega_\alpha, \omega_\beta, \omega_\gamma) = \left(\varphi, 0, \varphi - 1, 0, \pm 2\sqrt{\varphi - \varphi^2}, 0\right), \tag{2.17}$$

$$(\alpha, \beta, \gamma, \omega_\alpha, \omega_\beta, \omega_\gamma) = \left(\tfrac{1}{\sqrt{3}}, \tfrac{1}{\sqrt{3}}, \tfrac{1}{\sqrt{3}}, 0, 0, 0\right), \tag{2.18}$$

where ω_α, ω_β and ω_γ are the components of vorticity along the eigenvectors corresponding to the strain rates eigenvalues α, β and γ. The term φ is a free parameter which depends on initial conditions only. It is reasonable to conclude that these fixed points represent the turbulent velocity gradient behaviour in the limit of very large Mach number.

3. HEE normalization and conditional statistics

Inviscid incompressible velocity gradient dynamics exhibit finite-time singularity (Cantwell 1992; Girimaji & Speziale 1995) rendering numerical computations difficult. In this section, we first present the normalized version of HEE which circumvents the finite-time singularity problem by rescaling time. Then we proceed to describe the manner in which statistics are gathered and present the rationale for conditional averaging based on dilatational level.

3.1. *Normalization and rescaling*

We define the normalized velocity gradient tensor as

$$\boldsymbol{a}_{ij} \equiv \frac{\boldsymbol{A}_{ij}}{\epsilon} \quad \epsilon \equiv \sqrt{\boldsymbol{A}_{mn}\boldsymbol{A}_{mn}}. \tag{3.1a, b}$$

The quantity $\boldsymbol{a}_{ij}$ contains all the geometrical information about the velocity gradient tensor and has the advantage of being bounded ($-1 \leqslant a_{ij} \leqslant 1$). The substitution of $\boldsymbol{a}_{ij}$ in (2.13), however, results in the appearance of ϵ, which itself can diverge in finite time. To eliminate ϵ from the equations the evolution is considered in rescaled time t', such that $dt' \equiv dt/\tau$, where $\tau \equiv 1/\epsilon$. With these change of variables, (2.13) and (2.14) take the following form:

$$\frac{\mathrm{d}\boldsymbol{a}_{ij}}{\mathrm{d}t'} = \boldsymbol{a}_{ij}\boldsymbol{a}_{mn}\boldsymbol{a}_{kn}\boldsymbol{a}_{mk} + \tau^2\boldsymbol{a}_{ij}\boldsymbol{a}_{mn}\boldsymbol{P}_{mn} - \boldsymbol{a}_{ik}\boldsymbol{a}_{kj} - \tau^2\boldsymbol{P}_{ij}, \tag{3.2}$$

$$\frac{\mathrm{d}\tau}{\mathrm{d}t'} = \tau\boldsymbol{a}_{mn}\boldsymbol{a}_{kn}\boldsymbol{a}_{mk} + \tau^3\boldsymbol{a}_{mn}\boldsymbol{P}_{mn}, \tag{3.3}$$

$$\frac{\mathrm{d}\boldsymbol{P}_{ij}}{\mathrm{d}t'} = -\boldsymbol{P}_{ik}\boldsymbol{a}_{kj} - \boldsymbol{P}_{kj}\boldsymbol{a}_{ki} - (n-1)\boldsymbol{P}_{ij}\boldsymbol{a}_{kk}. \tag{3.4}$$

This set has the same number of equations as that of the unnormalized form. The equations are computationally well behaved even if the unnormalized velocity gradients diverge in finite time. The normalized equations (3.2)–(3.4) are now employed to examine velocity gradient geometry. As in Girimaji & Speziale (1995), time integration of (3.2)–(3.4) is performed using fourth-order Runge–Kutta scheme with a specified set of initial conditions for each realization or particle. A particle is 'created' by assigning randomly generated values for initial $\boldsymbol{A}_{ij}$. A random number generator that produces uniformly distributed numbers between -1 and 1 is employed for the purpose. Initial τ is set to unity for all particles. The initial $\boldsymbol{P}_{ij}$ is chosen as in the REE model

$$\boldsymbol{P}_{ij(t=0)} = -\frac{\boldsymbol{A}_{mn}\boldsymbol{A}_{nm}}{3}\delta_{ij}. \tag{3.5}$$

Starting from this initial condition, $\boldsymbol{P}_{ij}$ then evolves according to (3.4).

3.2. *On the nature of HEE*

The HEE, REE and Burgers velocity gradient models are all autonomous dynamical equation sets with one or more stable fixed point families. The evolution and asymptotic behaviour of the REE velocity gradients are described in detail in Cantwell (1992). The incompressibility constraint makes REE transient behaviour analytically tractable. The transient behaviour of Burgers and the HEE model do not appear to be as easily amenable to analytical examination. As mentioned earlier, the asymptotic behaviour of Burgers velocity gradient dynamics is given in Bikkani & Girimaji (2007). Our computations show (more on this in next section) that HEE, like Burgers, yields two distinct velocity gradient stable fixed points. Starting from specified initial conditions, a typical solution trajectory evolves rapidly with non-monotonic changes in dilatation and approaches one of the two fixed points in long times. While the asymptotic geometry of the velocity gradient tensor is important, the transient dynamics also yields crucial insight into turbulence processes. We characterize the transient dynamics conditioned upon the current value of normalized dilatation. Normalized dilatation quantifies the degree of compression of a fluid element, as it represents the rate of change of density. Velocity gradient statistics conditioned on dilatation provides a basis for comparison of HEE against DNS data.

To minimize the influence of initial conditions, statistics are gathered after an initial time lapse T

$$T = \frac{1}{(\tau\boldsymbol{a}_{mn}\boldsymbol{a}_{kn}\boldsymbol{a}_{mk} + \tau^3\boldsymbol{a}_{mn}\boldsymbol{P}_{mn})_{t'=0}}. \tag{3.6}$$

From (3.6) T can be seen as one velocity gradient turn-over time.

3.3. *Conditional statistics*

We perform HEE calculations with an ensemble of fluid particles in order to obtain statistics of various quantities of interest. The normalized velocity gradient tensor ($\boldsymbol{a}_{ij}$) is separated into its symmetric and anti-symmetric parts: the strain rate tensor ($\boldsymbol{s}_{ij}$) and the rotation rate tensor ($\boldsymbol{w}_{ij}$). The symbols α, β and γ are assigned to the three eigenvalues of $\boldsymbol{s}_{ij}$ such that $\alpha \geqslant \beta \geqslant \gamma$. The sum of these eigenvalues is the dilatation ($\boldsymbol{a}_{ii}$) or the measure of the rate of change in element volume. In compressible flows the normalized dilatation $\boldsymbol{a}_{ii}$ can vary within the algebraic limits of $-\sqrt{3}$ to $\sqrt{3}$. Expanding fluid elements are characterized by positive dilatation values whereas contracting ones by negative dilatation values. Ratios between the strain rate eigenvalues help in visualizing the change in shape of the fluid element. Each of the eigenvalues is normalized as follows:

$$\alpha^* = \frac{\alpha}{\sqrt{\alpha^2+\beta^2+\gamma^2}} \quad \beta^* = \frac{\beta}{\sqrt{\alpha^2+\beta^2+\gamma^2}} \quad \gamma^* = \frac{\gamma}{\sqrt{\alpha^2+\beta^2+\gamma^2}}. \quad (3.7a, b, c)$$

Another point of interest is the orientation of the vorticity vector, $\boldsymbol{\omega}$. This is examined in terms of the cosine of the angles that the vorticity vector makes with the eigenvectors of (i) the strain rate tensor and (ii) the pressure Hessian tensor $\boldsymbol{P}_{ij}$. Eigenvalues of the pressure Hessian tensor are represented by the symbols α_p, β_p and γ_p such that $|\alpha_p| \geqslant |\beta_p| \geqslant |\gamma_p|$ (Ohkitani & Kishiba 1995). We also examine the three invariants of the normalized velocity gradient tensor $\boldsymbol{a}_{ij}$. The definitions of these invariants are (Chong *et al.* 1990)

$$p \equiv -\boldsymbol{a}_{ii}, \quad (3.8a)$$

$$q \equiv \tfrac{1}{2}(p^2 - \boldsymbol{s}_{ij}\boldsymbol{s}_{ji} - \boldsymbol{w}_{ij}\boldsymbol{w}_{ji}), \quad (3.8b)$$

$$r \equiv \tfrac{1}{3}(-p^3 + 3pq - \boldsymbol{s}_{ij}\boldsymbol{s}_{jk}\boldsymbol{s}_{ki} - 3\boldsymbol{w}_{ij}\boldsymbol{w}_{jk}\boldsymbol{s}_{ki}). \quad (3.8c)$$

4. Results and discussion

In this section we compare the performance of the HEE model against some established analytical and numerical results. We first examine the asymptotic states of the HEE equation and discuss their relation to the stable fixed points of Burgers velocity gradient dynamics. Next we compare the performance of the HEE in the incompressible limit against incompressible turbulence DNS. Here we also make comparisons with REE results. Finally we compare HEE against compressible DNS results at various intermediate levels of dilatation.

4.1. *Asymptotic behaviour of HEE*

As mentioned earlier, the numerical integration of the HEE equations reveal two asymptotic states for the normalized velocity gradient tensor. The normalized dilatations of the two fixed points are approximately 1.7 and -1. All particles going to the fixed point with the normalized dilatation value of 1.7 have a vorticity-free three-dimensional isotropic expansion-wave structure

$$(\alpha, \beta, \gamma, \omega_\alpha, \omega_\beta, \omega_\gamma) \approx \left(\tfrac{1}{\sqrt{3}}, \tfrac{1}{\sqrt{3}}, \tfrac{1}{\sqrt{3}}, 0, 0, 0\right).$$

For all the particles in this asymptotic state we observe that the inertial term is much larger than the pressure term $\|\boldsymbol{A}_{ik}\boldsymbol{A}_{kj}\| \gg \|\boldsymbol{P}_{ij}\|$ referring to (2.13). Clearly, this is a pressure-released limit of the HEE. It is then reasonable to compare this solution to

the pressure-released Navier–Stokes (Burgers turbulence) fixed point behaviour given in (2.17) and (2.18). This HEE pressure-released fixed point is identical to (2.18).

All particles reaching the other asymptotic state ($\boldsymbol{a}_{ii} = -1$) have one-dimensional compression wave-like structure with negligible vorticity

$$(\alpha, \beta, \gamma, \omega_\alpha, \omega_\beta, \omega_\gamma) \approx (0, 0, -1, 0, 0, 0).$$

This solution happens to be a special case of the first fixed point (2.17) of Burgers dynamics with parameter $\varphi = 0$. Despite this agreement we do not classify this HEE asymptotic state as a pressure-released behaviour. Our computations show that in this asymptotic state the inertia terms are not convincingly large enough as compared to the pressure terms ($\|\boldsymbol{A}_{ik}\boldsymbol{A}_{kj}\| \approx 5\,\|\boldsymbol{P}_{ij}\|$).

Overall, it can be concluded that in the pressure-released or high-Mach-number limit the HEE reproduces asymptotic Burgers turbulence behviour.

4.2. *HEE in incompressible limit*

Now we will examine HEE for the other limiting case, incompressible turbulence. The HEE results conditioned upon zero dilatation can be interpreted as the incompressible-limit behaviour of the HEE model. We compare this behaviour against DNS results of incompressible decaying isotropic turbulence (Kerimo & Girimaji 2007). We also include the asymptotic REE results in this discussion to highlight the relative improvements achieved with the HEE model in predicting incompressible turbulence behaviour.

Alignment of vorticity vector with respect to the eigenvectors of the strain rate tensor is of much physical significance as it quantifies the extent of vortex stretching in turbulent flows. The information about the sign and magnitude of strain-rate eigenvalues helps us understand cascading due to self straining. In figures 1 and 2 we present probability density functions of the normalized strain rate eigenvalues (α^*, β^*, γ^*) and the cosine of the angles vorticity makes with the corresponding eigenvectors. While the probability density functions completely describe the distributions of the quantities of interest, the peaks can be interpreted as the most probable values. The success of asymptotic REE has been limited to qualitatively predicting the following two most probable features of incompressible turbulence: (i) the intermediate eigenvalue is small but positive and (ii) vorticity aligns best with the eigenvector corresponding to the intermediate eigenvalue. The REE probability density functions do not recover the broad distributions seen in DNS. The HEE model, on the other hand, not only reproduces the most probable values seen in DNS but recovers the entire range of distributions in figures 1 and 2.

Next, we compare joint distribution of the second and third invariants of a_{ij} (3.8). The associated topology of the velocity gradient tensor can be inferred with knowledge of the coordinates (q, r) on the $p = 0$ plane for incompressible flows (Chong *et al.* 1990). Chen *et al.* (1990) and Soria *et al.* (1994) investigate the dominant local topologies at the dissipating scales of motion in mixing layers in terms of the invariants. Soria *et al.* (1994) plot joint number density of unnormalized invariants rather than joint probability density function. The joint probability density function of q and r computed from isotropic decay DNS data (figure 3*a*) has two prominent features: (i) significant amount of data lies in the lower-right quadrant concentrated along the curve $q = -\sqrt[3]{27r^2/4}$ (Vieillefosse line) and (ii) bulk of data lies almost uniformly distributed over a roughly elliptical region in the upper-left quadrant. These features have been observed in DNS of a variety of flows and are fairly independent of initial conditions (Chen *et al.* 1990; Soria *et al.* 1994). The local

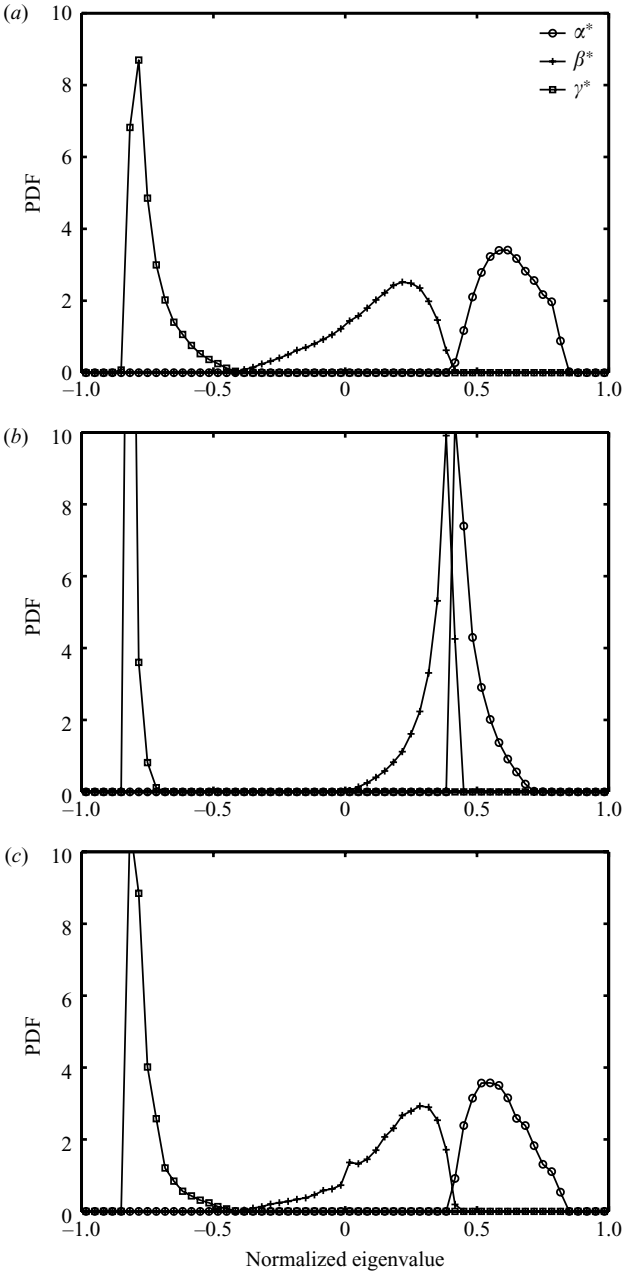

FIGURE 1. Probability density functions of normalized strain rate eigenvalues (α^*, β^*, γ^*). (*a*) Incompressible DNS, (*b*) asymptotic REE and (*c*) zero-dilatation HEE.

topologies corresponding to the distributions in the upper-left and the lower-right quadrants are stable focus stretching and unstable node saddle–saddle. While the asymptotic REE does capture the first feature seen in DNS, it completely fails to recover the second. The asymptotic REE joint probability density function is completely concentrated on the curve $q = -\sqrt[3]{27r^2/4}$ (figure 3*b*). Failure to show any topology in the upper-left quadrant has been one of the major shortcomings of the

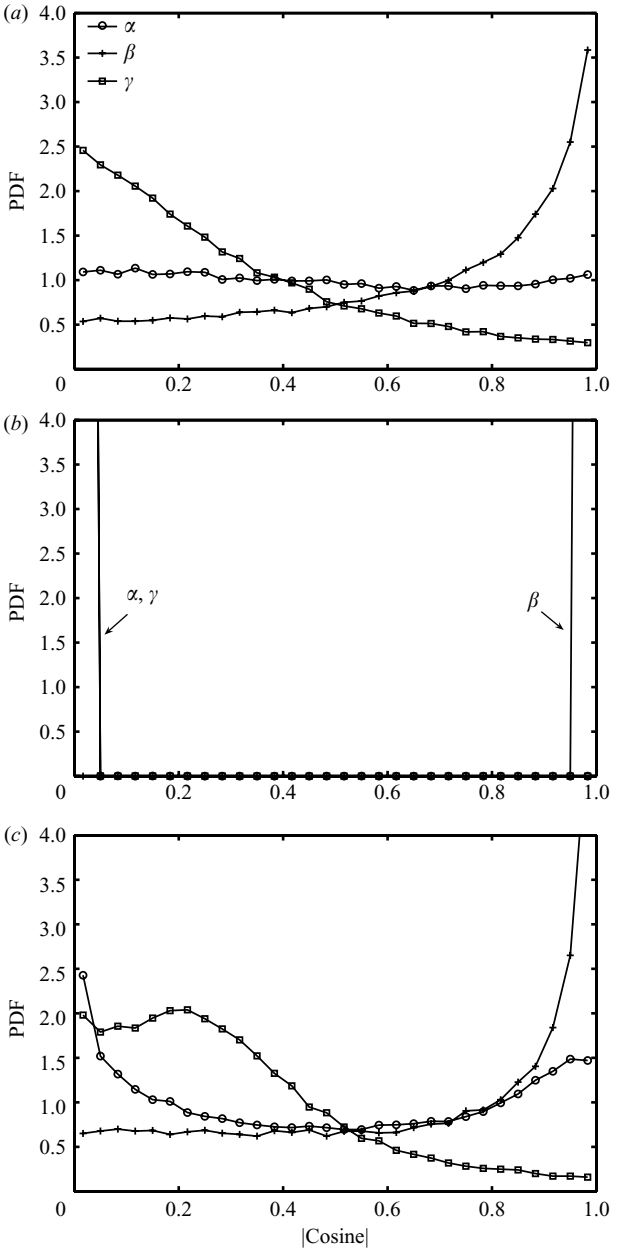

FIGURE 2. Probability density functions of the cosines (magnitude) of the angles between vorticity and strain rate eigenvectors. (*a*) Incompressible DNS, (*b*) asymptotic REE and (*c*) zero-dilatation HEE.

REE model, and it has attracted considerable research attention (Cantwell 1993; Chevillard & Meneveau 2006). The HEE model on the other hand convincingly recovers both the aforementioned features of the $q-r$ distribution seen in DNS (see figure 3*c*). Evidently, the HEE results conditioned on zero dilatation capture the richness of topology observed in incompressible flows much better than the asymptotic REE results.

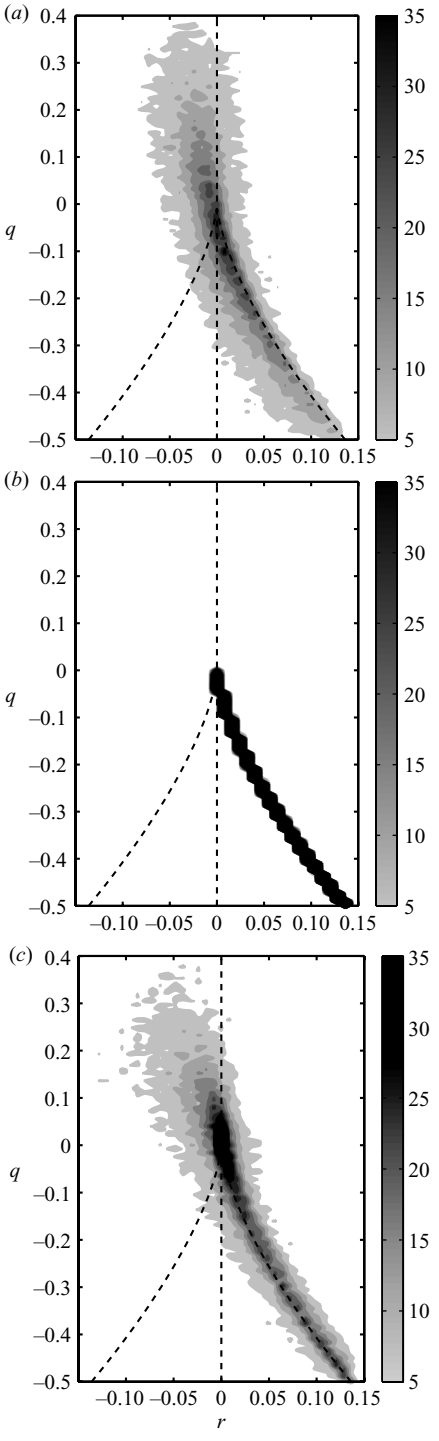

FIGURE 3. Joint probability density function of the second and third invariants (q, r). (*a*) Incompressible DNS, (*b*) asymptotic REE and (*c*) zero-dilatation HEE.

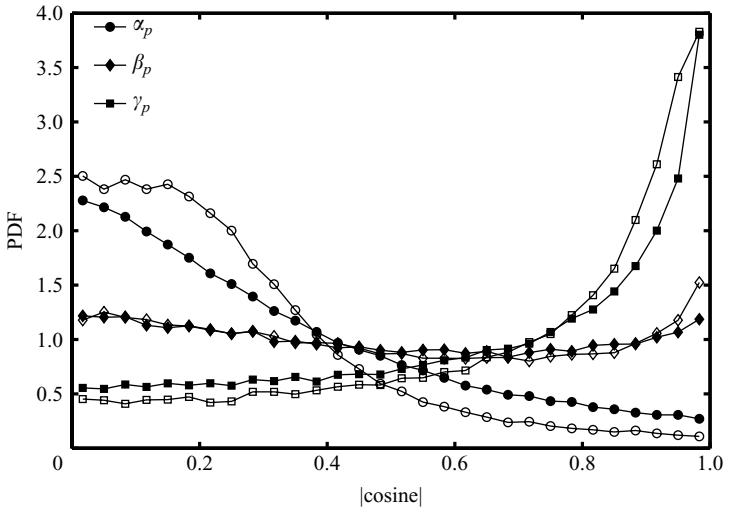

FIGURE 4. Probability density functions of the cosines (magnitude) of the angles between vorticity and pressure Hessian eigenvectors. Closed symbols: incompressible DNS. Open symbols: zero-dilatation HEE.

It is reasonable to attribute the observed superiority of HEE over REE to the inclusion of anisotropic portion of the pressure Hessian tensor. We can further validate the HEE model by examining how vorticity is oriented with respect to the eigenvectors of the pressure Hessian tensor. Eulerian analysis of incompressible flows (Ohkitani & Kishiba 1995) suggests that at points of maximum enstrophy, vorticity aligns with the eigenvector of the pressure Hessian tensor associated with the smallest eigenvalue magnitude. Based on this insight we categorize the pressure Hessian eigenvalues as α_p, β_p and γ_p such that $|\alpha_p| \geqslant |\beta_p| \geqslant |\gamma_p|$. This basis of categorization is different from the one followed by Kalelkar (2006), wherein the pressure Hessian eigenvalues are categorized by arranging them simply in descending order of value. In figure 4 we plot the probability density functions of the cosine of the angles between vorticity and pressure Hessian eigenvectors. Similar to what has been observed by Ohkitani & Kishiba (1995) in inviscid flows, the DNS also shows a distinct preference of vorticity to align with the eigenvector of γ_p – the eigenvalue with the smallest magnitude. The HEE model accurately recovers not only this trend but the entire distributions seen in DNS. It should be noted that the REE model has an isotropic pressure Hessian tensor and hence does not lend itself to this important examination.

Based on the foregoing discussion we summarize that the HEE model in its incompressible limit accurately recovers the incompressible turbulence behaviour seen in DNS. Moreover, with a more accurate description of the pressure Hessian tensor, the HEE model shows significant improvements over the REE model.

4.3. *HEE at intermediate dilatations*

Having established that the HEE model captures the turbulence behaviour reasonably well in the extreme Mach number limits, we now examine its validity at intermediate levels of dilatation. The model results will now be compared against decaying compressible isotropic turbulence DNS data. Although the model development invokes the isentropic assumption, we would like to compare it against general non-isentropic turbulence. Therefore, the decaying turbulence initial conditions are as given in Lee (2008) rather than Ristorcelli & Blaisdell (1997), which is expressly for

isentropic turbulence. As is standard procedure in REE literature, we compare DNS data against HEE results obtained from statistically unbiased randomly generated velocity gradient initial conditions. As the HEE equations constitute a nonlinear dynamical system, the asymptotic velocity gradient structure will be independent of the initial condition. We do expect the levels of dilatational kinetic energy and dilatational dissipation to depend on initial conditions and initial turbulent Mach number (Blaisdell, Mansour & Reynolds 1993; Lee 2008). However, the velocity gradient structure conditioned on local dilatation is expected to be weakly dependent on initial conditions and turbulent Mach number (Lee 2008). To ensure that initial conditions do not unduly influence the model-data comparison, the HEE statistics are gathered only after finite time-elapse corresponding to several turn-over times. We would like to point out at the very outset that this comparison between non-isentropic DNS and HEE results from randomly generated initial conditions constitute a very rigorous test of the proposed model.

As in REE, in HEE velocity gradient tensor is computed following a fluid particle. In addition, in HEE, pressure Hessian is also computed explicitly from an evolution equation. Both in REE and HEE the velocity field is not considered and hence the kinetic energy evolution cannot be computed. Since REE and HEE are inviscid models, dissipation is also not known. Hence, DNS and HEE comparison is restricted to velocity gradient alignment angles and invariant maps (Vieillefosse 1982, Ashurst *et al.* 1987, Cantwell 1992, 1993).

The HEE computations of the probability density functions of the strain rate eigenvalues are compared against decaying compressible turbulence DNS data of Lee (2008). The DNS velocity gradient statistics are computed at the peak of dissipation in a simulation with initial values of turbulent Mach number and Taylor-scale Reynolds number of 0.88 and 55.6, respectively. The probability density functions are conditioned on various values of a_{ii} ranging from -1.4 to 1.65. Figures 5(*a*), 6(*a*) and 7(*a*) show the probability density functions of the normalized eigenvalues (α^*, β^* and γ^*) computed from DNS data. Each of these probability density functions is a single-peaked distribution with a moderate spread around the peak. For example, the probability density function of the largest eigenvalue conditioned on $a_{ii} = -1.4$ has a peak at $\alpha^* = -0.15$ with a spread in the range $-0.4 < \alpha^* < 0.1$.

The DNS probability density functions of the intermediate eigenvalue (β^*) shift monotonically from left to right as a_{ii} increases. The corresponding shifts for the largest (α^*) and the smallest (γ^*) eigenvalues are non-monotonic. The arrows placed on the corresponding figures indicate the direction of these shifts with increasing a_{ii}. For the largest eigenvalue, the reversal in the direction of shift happens at a high positive a_{ii}, whereas for the smallest eigenvalue the reversal happens at a high negative a_{ii}. All these features observed in DNS are very well recovered by HEE in figures 5(*b*), 6(*b*) and 7(*b*). Remarkably, the values of dilatation at which the trends reverse are captured very accurately by HEE.

Next we compare the shapes of the probability density functions. It is clear that the HEE does not recover exactly the shapes of the probability density functions seen in DNS. However, there are some ranges of a_{ii} over which the agreement is good. For the largest eigenvalue the HEE distributions become increasingly more accurate as a_{ii} approaches higher positive values. The HEE probability density functions for the intermediate eigenvalue are fairly close to their DNS counterparts at moderately-negative and moderately-positive dilatations. The distinct asymmetry of the β^* probability density functions seen in DNS at moderate dilatations is well

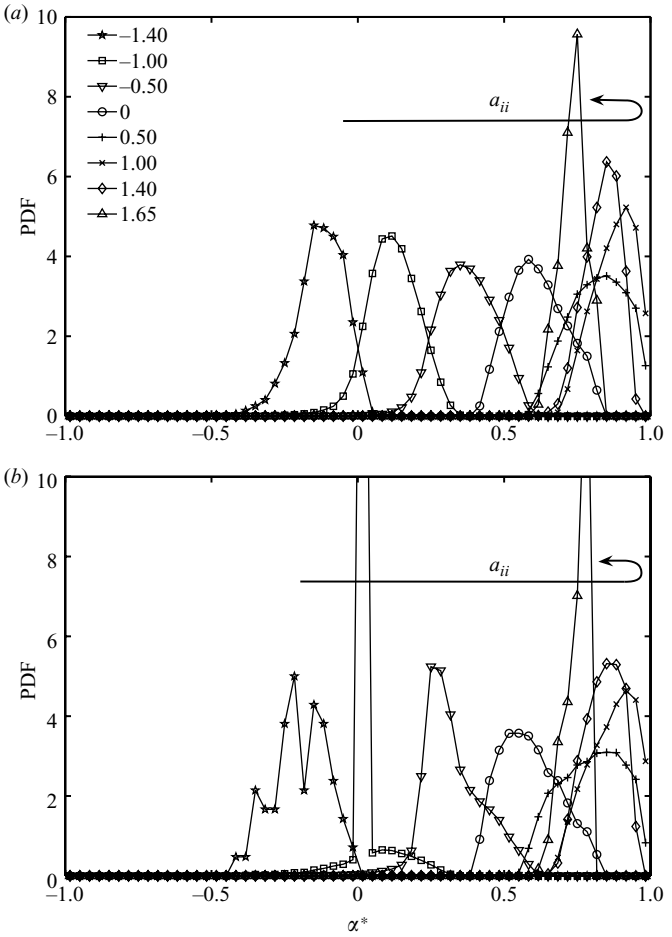

FIGURE 5. Probability density functions of normalized largest strain rate eigenvalue (α^*) conditioned on various values of a_{ii}. (*a*) Compressible DNS and (*b*) HEE.

reproduced by HEE. For the smallest eigenvalue the agreement between the DNS and HEE distributions gets better at highly-negative dilatations.

With figure 8 we take a closer look at the dependence of most probable strain rate eigenvalues (peaks of the probability density functions included in figures 5–7) on normalized dilatation. The agreement between the HEE and DNS values is generally good with an exception at $a_{ii} = -1$. At this dilatation the HEE computations show that the strain rate tensor is under severe uni-axial compression with $(\alpha^*, \beta^*, \gamma^*) \approx (0.02, 0.02, -0.98)$, which is somewhat different from the DNS behaviour $[(\alpha^*, \beta^*, \gamma^*) \approx (0.12, -0.15, -0.98)]$. One of the possible reasons for this discrepancy could be the role of viscosity. HEE computations reveal that almost all contracting particles with $a_{ii} = -1$ are associated with very large velocity gradient magnitudes and hence sizable viscous effects. It is plausible that dissipation and viscous effects would dominate the dynamics in these regions. In these high dissipation regions, the isentropic assumption is also questionable.

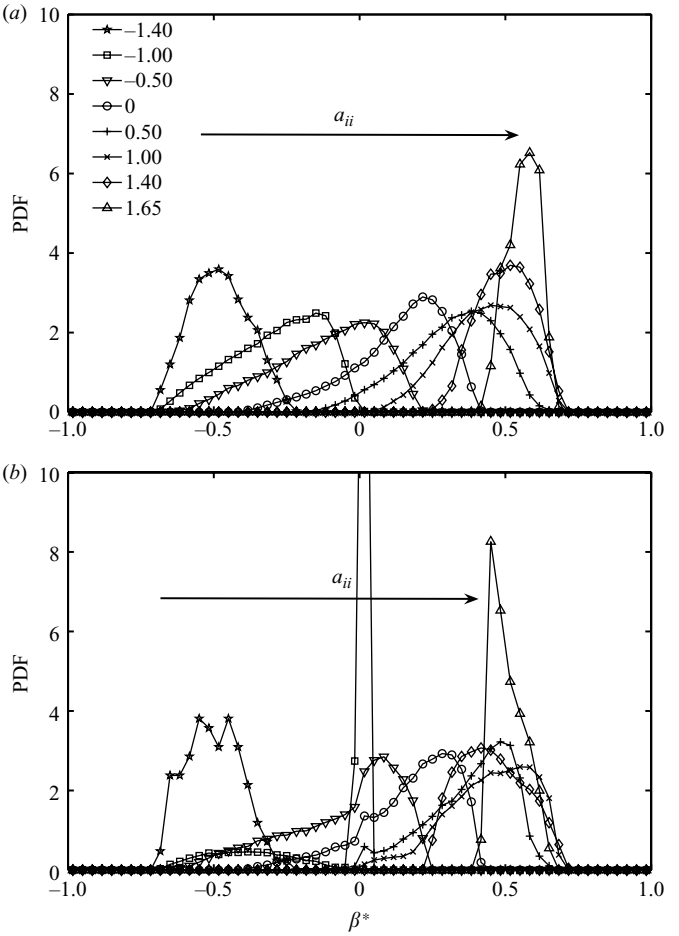

FIGURE 6. Probability density functions of normalized intermediate strain rate eigenvalue (β^*) conditioned on various values of a_{ii}. (*a*) Compressible DNS and (*b*) HEE.

5. Conclusions

Under the assumptions of uniform velocity gradients in an inviscid compressible and isentropic flow field we develop a model – the homogenized Euler equation – for describing compressible velocity gradient dynamics. The medium is assumed to be a calorically perfect gas. Coupling between the energy and momentum equation is invoked through the perfect gas state and energy equations. The pressure Hessian evolves as dictated by thermodynamic considerations. In contrast to the restricted Euler equation, the anisotropic pressure Hessian effects are retained intact in this approach. The model comprises of 15 ordinary differential equations in 15 unknowns. Computations are performed for an ensemble of random initial velocity gradient tensors. We study various statistics pertaining to the structure of the velocity gradient tensor conditioned upon normalized dilatation. HEE results in the incompressible limit compare very well against DNS results of incompressible decaying isotropic turbulence. Moreover, in this limit the HEE computations are much improved over the asymptotic REE results. At various non-zero dilatations the HEE very well captures many features of the principal strain rate statistics seen in compressible DNS. The

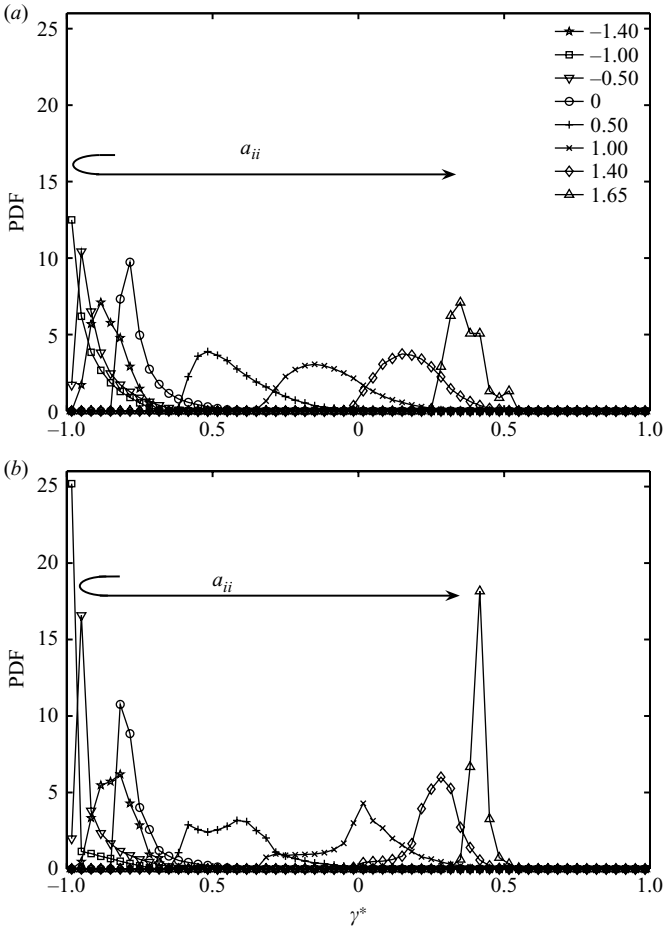

FIGURE 7. Probability density functions of normalized smallest strain rate eigenvalue (γ^*) conditioned on various values of a_{ii}. (*a*) Compressible DNS and (*b*) HEE.

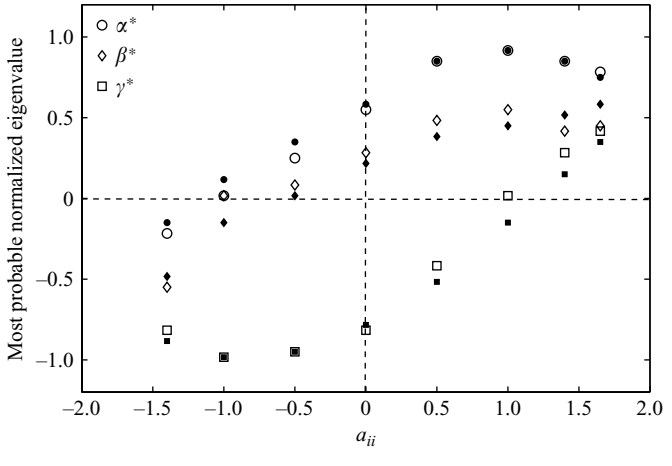

FIGURE 8. Most probable normalized strain rate eigenvalues (α^*, β^*, γ^*) versus a_{ii}. Closed symbols: Compressible DNS. Open symbols: HEE.

HEE behviour in the high-Mach-number (pressure-released) limit is consistent with Burgers velocity gradient dynamics. The HEE is put forward as a useful model to describe velocity gradient dynamics in compressible turbulence.

This work was supported by AFOSR (MURI) Grant No. FA9550-04-1-0425 (Program Manager: Dr John Schmisseur).

REFERENCES

Ashurst, W. T., Kerstein, A. R., Kerr, R. M. & Gibson, C. H. 1987 Alignment of vorticity and scalar gradient with strain rate in simulated Navier–Stokes turbulence. *Phys. Fluids* **30**.

Avellaneda, M., Ryan, R. & Weinan, E. 1995 Pdfs for velocity and velocity gradients in burgers turbulence. *Phys. Fluids* **7**.

Bikkani, R. & Girimaji, S. S. 2007 Role of pressure in non-linear velocity gradient dynamics in turbulence. *Phys. Rev.* E **75**.

Blaisdell, G. A., Mansour, N. N. & Reynolds, W. C. 1993 Compressibility effects on the growth and structure of homogenous turbulent shear flow. *J. Fluid Mech.* **256**, 443–485.

Bouchaud, J.-P. & Mzard, M. 1996 Velocity fluctuations in forced burgers turbulence. *Phys. Rev.* E **54**.

Cantwell, B. J. 1992 Exact solution of a restricted euler equation for the velocity gradient tensor. *Phys. Fluids* A **4**.

Cantwell, B. J. 1993 On the behavior of velocity gradient tensor invariants in direct numerical simulations of turbulence. *Phys. Fluids* A **5**.

Chen, J. H., Chong, M. S., Soria, J., Sondergaard, R., Perry, A. E., Rogers, M., Moser, R. & Cantwell, B. J. 1990 A study of the topology of dissipating motions in direct numerical simulations of time-developing compressible and incompressible mixing layers. In *Proceedings of the Center for Turbulence Research Summer Program, CTR-S90.*

Chertkov, M., Pumir, A. & Shraiman, B. I. 1999 Lagrangian tetrad dynamics and phenomenology of turbulence. *Phys. Fluids* **11**.

Chevillard, L. & Meneveau, C. 2006 Lagrangian dynamics and statistical geometric structure of turbulence. *Phys. Rev. Lett.* **97**.

Chong, M. S., Perry, A. E. & Cantwell, B. J. 1990 A general classification of three-dimensional flow fields. *Phys. Fluids* A **2**.

Girimaji, S. S. & Pope, S. B. 1990 A diffusion model for velocity gradients in turbulence. *Phys. Fluids* A **2**.

Girimaji, S. S. & Speziale, C. G. 1995 A modified restricted euler equation for turbulent flows with mean velocity gradients. *Phys. Fluids* **7**.

Girimaji, S. S. & Zhou, Y. 1995 Spectrum and energy transfer in steady burgers turbulence. *Phys. Lett.* A **202**.

Jeong, E. & Girimaji, S. S. 2003 Velocity-gradient dynamics in turbulence: effect of viscosity and forcing. *Theor. Comput. Fluid Dyn.* **16**, 421–432.

Kalelkar, C. 2006 Statistics of pressure fluctuations in decaying isotropic turbulence. *Phys. Rev.* E **73**.

Kerimo, J. & Girimaji, S. S. 2007 Boltzmann – BGK approach to simulating weakly compressible turbulence: comparison between lattice Boltzmann and gas kinetic methods. *J. Turbul.* **8**, N 46.

Lee, K. 2008 Heat release effects on decaying homogeneous compressible turbulence. PhD thesis, Texas A & M University.

Li, Y. & Meneveau, C. 2005 Origin of non-Gaussian statistics in hydrodynamic turbulence. *Phys. Lett.* **95**.

Ohkitani, K. 1993 Eigenvalue problems in 3D Euler flows. *Phys. Fluids* A **5**.

Ohkitani, K. & Kishiba, S. 1995 Non-local nature of vortex stretching in an inviscid fluid. *Phys. Fluids* **7**.

Passot, T. & Vzquez-Semadeni, E. 1998 Density probability distribution in one-dimensional polytropic gas dynamics. *Phys. Rev.* E **58**.

Perry, A. E. & Chong, M. S. 1987 A description of eddying motion and flow patterns using critical point concepts. *Ann. Rev. Fluid Mech.* **19**, 125–155.

Ristorcelli, J. R. & Blaisdell, G. A. 1997 Consistent initial conditions for the DNS of compressible turbulence. *Phys. Fluids* **9** (1).

Soria, J., Sondergaard, R., Cantwell, B. J., Chong, M. S. & Perry, A. E. 1994 A study of the fine-scale motions of incompressible time-developing mixing layers. *Phys. Fluids* **6**.

Vieillefosse, P. 1982 Local interaction between vorticity and shear in a perfect incompressible fluid. *J. Phys. (Paris)* **43**, 837.